

Strategy to measure tau $g - 2$ via photon fusion in LHC proton collisions

Lydia Beresford,^{1,*} Savannah Clawson,^{1,†} and Jesse Liu^{2,‡}

¹*Deutsches Elektronen-Synchrotron DESY, Notkestr. 85, 22607 Hamburg, Germany*

²*Cavendish Laboratory, University of Cambridge, Cambridge CB3 0HE, UK*

Measuring the tau-lepton (τ) anomalous magnetic moment $a_\tau = (g_\tau - 2)/2$ in photon fusion production ($\gamma\gamma \rightarrow \tau\tau$) tests foundational Standard Model principles. However, $\gamma\gamma \rightarrow \tau\tau$ eludes observation in LHC proton collisions (pp) despite enhanced new physics sensitivity from higher-mass reach than existing probes. We propose a novel strategy to measure $pp \rightarrow p(\gamma\gamma \rightarrow \tau\tau)p$ by introducing the overlooked electron-muon signature with vertex isolation for signal extraction. Applying the effective field theory of dipole moments, we estimate 95% CL sensitivity of $-0.0092 < a_\tau < 0.011$ assuming 300 fb^{-1} luminosity and 5% systematics. This fourfold improvement beyond existing constraints opens a crucial path to unveiling new physics imprinted in tau-lepton dipoles.

I. INTRODUCTION

Precise measurements of electromagnetic (EM) dipoles are fundamental tests of the Standard Model (SM) that could reveal beyond-the-SM (BSM) physics. A cornerstone SM principle is lepton universality, where all three generations (electron e , muon μ , tau-lepton τ) couple equally to gauge bosons. The leading SM loop correction from quantum fluctuations is also flavor universal, shifting magnetic moments by the Schwinger term $\alpha_{\text{EM}}/2\pi \simeq 0.0012$ [1, 2]. The electron and muon anomalous magnetic moments $a_{e,\mu} = (g_{e,\mu} - 2)/2$ are now tested to 13 [3–12] and 10 decimal places [13–16], respectively. However, the tau-lepton counterpart a_τ is still compatible with zero to two decimal places [17] as its 0.3 ps proper lifetime [18–21] precludes storage-ring probes [15]. The existence of tau-lepton loop interactions with photons in nature thus remains strikingly untested.

The most precise single-experiment a_τ constraint is a $-0.052 < a_\tau^{\text{obs}} < 0.013$ 95% CL limit by DELPHI [22] at the Large Electron Positron Collider (LEP), with similar precision by L3 and OPAL [23, 24]. ATLAS and CMS recently pioneered Large Hadron Collider (LHC) probes of a_τ using photon fusion production of tau-leptons ($\gamma\gamma \rightarrow \tau\tau$) in lead-lead (PbPb) data [25, 26]; the ATLAS 95% CL limit is $-0.057 < a_\tau^{\text{obs}} < 0.024$. Such large experimental uncertainties relative to the SM prediction $a_{\tau,\text{SM}}^{\text{pred}} = 0.00117721(5)$ [27] could conceal BSM dynamics motivated by lepton sector tensions [28–44]. Specific models predict quadratic scaling $\delta a_\ell \propto m_\ell^2$ with lepton mass m_ℓ [45–47], implying $(m_\tau/m_\mu)^2 \simeq 280$ times larger effects for a_τ than a_μ . New physics can also violate charge-parity (CP) symmetry, inducing an electric dipole d_τ . Standard LHC proton-proton (pp) collisions reach higher $\mathcal{O}(\text{TeV})$ masses, enhancing BSM dipole sensitivity over $\mathcal{O}(100 \text{ GeV})$ in PbPb [48–53]. Despite this key benefit, cross-section yielding over 30 million events to date, and major photon-fusion advances [54–88], $\gamma\gamma \rightarrow \tau\tau$ remarkably evades observation in pp data.

This paper proposes the strategy to measure $\gamma\gamma \rightarrow \tau\tau$ and tau-lepton EM dipoles in LHC pp collisions (Fig. 1). We initiate the first Monte Carlo (MC) simulation analysis of the $pp \rightarrow p(\gamma\gamma \rightarrow \tau\tau)p$ signal that includes im-

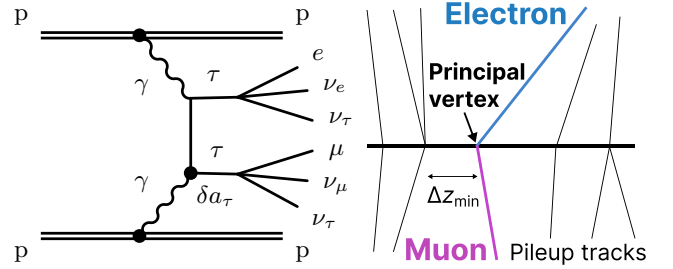


FIG. 1. Tau-leptons produced from photon fusion in proton beams with electron-muon $\tau\tau \rightarrow e\nu\mu\nu$ decays as a Feynman diagram (left) and detector signature illustrating the vertex isolation technique for the electron-muon vs pileup tracks (right). New physics can modify the magnetic moment δa_τ .

portant weak-boson backgrounds and detector effects neglected in earlier work [89]. Prevailing wisdom targets hadronic tau-lepton decays for high signal rates, but inefficient triggers, formidable backgrounds, and multiple pp interactions (pileup) obstruct detection. We overcome these longstanding obstacles by leveraging recent progress [90–92] to introduce the overlooked electron-muon signature, track-vertex isolation techniques (Fig. 1, right), and kinematic discriminants all unexplored for pp probes of $\gamma\gamma \rightarrow \tau\tau$. This unlocks crucial access to high-momentum kinematics unique to pp events that augment BSM dipole sensitivity. We also propose critical strategies for controlling systematics. Our proposal complements other production modes [93–98] and future facilities [99–112], while broadening the precision tau-lepton [113–119] and search programs [120–131].

II. MODEL AND SIMULATION

Relativistic field theory generalizes the Schrödinger-Pauli Hamiltonian $\mathcal{H} = -\boldsymbol{\mu}_\tau \cdot \mathbf{B} - \mathbf{d}_\tau \cdot \mathbf{E}$ describing EM dipoles into an effective Lagrangian coupling the Dirac spinor tensor $\sigma^{\mu\nu} = i[\gamma^\mu, \gamma^\nu]/2$ to the photon field $F_{\mu\nu}$

$$\mathcal{L}_{\text{dipole}} = \frac{1}{2} \bar{\tau}_L \sigma^{\mu\nu} \left(a_\tau \frac{e}{2m_\tau} - i d_\tau \gamma_5 \right) \tau_R F_{\mu\nu}, \quad (1)$$

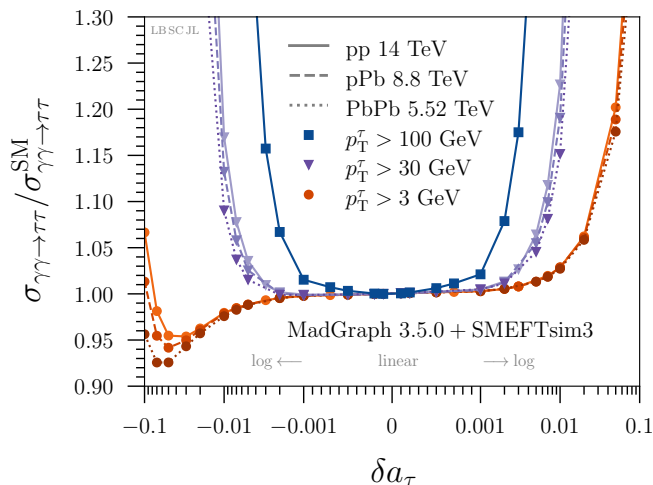


FIG. 2. Cross-sections relative to the SM $\sigma_{\gamma\gamma\rightarrow\tau\tau}/\sigma_{\gamma\gamma\rightarrow\tau\tau}^{\text{SM}}$ for elastic $\gamma\gamma \rightarrow \tau\tau$ production vs magnetic moment variations δa_τ with proton-proton pp 14 TeV (solid), proton-lead pPb 8.8 TeV (dashed), lead-lead PbPb 5.52 TeV (dotted) beams given tau-lepton transverse momentum $p_T^\tau > 100$ GeV (squares, only pp), 30 GeV (triangles), 3 GeV (circles).

where $\tau_{L(R)}$ is the left- (right-) handed tau-lepton spinor and γ^5 satisfies the $\{\gamma^5, \gamma^\mu\} = 0$ anticommutator. Quantum electrodynamics (QED) predicts a vanishing electric dipole $d_\tau = 0$ and vacuum fluctuations induce $a_\tau \neq 0$.

New physics at high-mass scale Λ can shift EM dipoles beyond SM values at low momentum transfers q satisfying $q^2 \ll \Lambda^2$, parameterized by SM Effective Field Theory (SMEFT) [132]. Following Ref. [49], we introduce the dimension-six SMEFT operator

$$\mathcal{L}_{\text{SMEFT}} = (C_{\tau B}/\Lambda^2) \bar{L}_\tau \sigma^{\mu\nu} \tau_R H B_{\mu\nu} \quad (2)$$

that modifies (a_τ, d_τ) at tree level [99], where L_τ (H) is the tau-lepton (Higgs) doublet, $B_{\mu\nu}$ is the hypercharge field, and $C_{\tau B}$ is a dimensionless, complex Wilson coefficient in the Warsaw basis [133]. We implement Eq. (2) in FEYNRULES [134] using the SMEFTsim_general_alphaScheme_UF0 model in SMEFTSIM 3.0.2 [135, 136]. The real (ceBRe33) and imaginary (ceBIm33) parts of $C_{\tau B}$ in the restrict_SMLimit_massless parameter card map to dipole shifts

$$\delta a_\tau = \frac{2m_\tau}{e} \frac{\text{Re}[C_{\tau B}]}{M}, \quad \delta d_\tau = \frac{\text{Im}[C_{\tau B}]}{M}, \quad (3)$$

defining $M = \Lambda^2/(\sqrt{2}v \cos \theta_W)$ in terms of the Weinberg angle θ_W and $v = 246$ GeV, $m_\tau = 1.776$ GeV, and $e = 1/\sqrt{4\pi}$ in Heaviside-Lorentz units. We interface SMEFTSIM with MADGRAPH 3.5.0 [137, 138] for cross-section calculation and MC event simulation.

Canonical calculations of LHC photon-fusion cross-sections $\sigma_{\gamma\gamma\rightarrow\tau\tau}^{(\text{pp})}$ factorize into convolutions of the elemen-

tary cross-section $\hat{\sigma}_{\gamma\gamma\rightarrow\tau\tau}$ with the photon flux $n(x)$ [139]

$$\sigma_{\gamma\gamma\rightarrow\tau\tau}^{(\text{pp})} = \int dx_1 dx_2 n(x_1)n(x_2) \hat{\sigma}_{\gamma\gamma\rightarrow\tau\tau}, \quad (4)$$

where $x_i = E_i/E_{\text{beam}}$ is the photon energy E_i emitted from proton i normalized to beam energy E_{beam} . We adopt the charge form factor (ChFF) flux from GAMMA-UPC 1.0 [140], which includes nonfactorizable soft-survival corrections to Eq. (4). The cross-section is proportional to the amplitude squared $\hat{\sigma}_{\gamma\gamma\rightarrow\tau\tau} \propto |\mathcal{A}|^2$,

$$|\mathcal{A}|^2 = |\mathcal{A}_{\text{SM}}|^2 + 2\text{Re}(\mathcal{A}_{\text{SM}}\mathcal{A}_{\text{BSM}}^*) + |\mathcal{A}_{\text{BSM}}|^2. \quad (5)$$

Generating $\gamma\gamma \rightarrow \tau\tau$ events with up to two EFT vertices models this SM-BSM quantum interference. The correspondence to static EM dipoles formally applies in the real photon limit $q_\gamma^2 \rightarrow 0$, satisfied for elastic photons from LHC protons $q_\gamma^2/m_\tau^2 \simeq (280 \text{ MeV}/1776 \text{ MeV})^2 \ll 1$.

We find the 14 TeV cross-section $\sigma_{\gamma\gamma\rightarrow\tau\tau}^{(\text{pp})}$ for elastic $\gamma\gamma \rightarrow \tau\tau$ production is 150 pb, yielding 4.5×10^7 events at 300 fb $^{-1}$ luminosity. Imposing transverse momentum $p_T^\tau > 30$ (100) GeV, the 100 (2.5) fb cross-section yields favorable 3×10^4 (750) events at 300 fb $^{-1}$, whereas the 25 nb (5.1 pb) PbPb cross-section yields fewer (negligible) 100 (0.02) events at 4 nb $^{-1}$. Figure 2 shows the relative cross-section variations versus δa_τ , assuming $\delta d_\tau = 0$ for different beams and minimum p_T^τ . Requiring $p_T^\tau > 30$ (100) GeV modifies $\sigma_{\gamma\gamma\rightarrow\tau\tau}^{(\text{pp})}$ by a measurable 5% for per-mille $\delta a_\tau = 0.005$ (0.001) shifts, dramatically improving δa_τ sensitivity when probing scales only accessible to pp beams. We generate around 2 million elastic $\gamma\gamma \rightarrow \tau\tau$ events per point for 27 coupling variations in the range $\delta a_\tau \in [-0.015, 0.015]$ with $\delta d_\tau = 0$, requiring $p_T^\tau > 15$ GeV in MADGRAPH and fully leptonic decays using PYTHIA 8.306 [141, 142] customized for photon fusion [91, 143] to improve MC statistics. Dissociative photon-fusion (indicated by p*) and background simulation follows standard MADGRAPH+PYTHIA procedures [138, 144, 145] detailed in Appendix 1, generating at least 1 million events per process. All samples have DELPHES 3.5.0 [146] detector emulation applied. We assume 300 fb $^{-1}$ for the 13–13.6 TeV dataset and 4000 fb $^{-1}$ for the 14 TeV High-Luminosity LHC (HL-LHC) [147]; Appendix 3 shows minor differences between these energies so we generate only 14 TeV MC for simplicity.

III. ANALYSIS PROPOSAL

We propose targeting the $\tau\tau \rightarrow e\nu\mu\nu$ decay with $2 \times \mathcal{B}(\tau \rightarrow e\nu) \times \mathcal{B}(\tau \rightarrow \mu\nu) \simeq 6\%$ [17] branching ratio. We emulate standard dilepton triggers selecting this signature by requiring the electron (muon) satisfy current offline thresholds $p_T^{e(\mu)} > 18$ (15) GeV [148–151] and tracker acceptance $|\eta_{e,\mu}| < 2.5$. After this selection, several backgrounds mimic this signal, which we denote *reducible* (*irreducible*) if they vanish (persist) in the

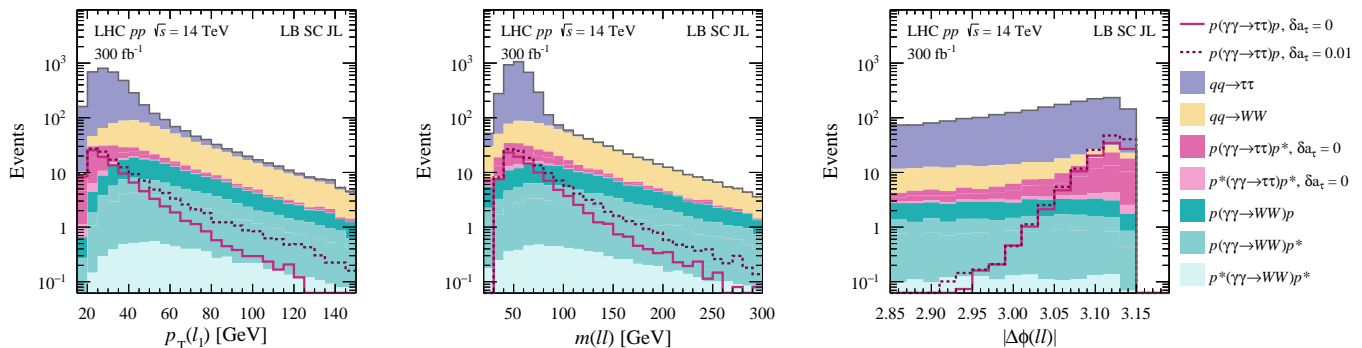


FIG. 3. Distributions normalized to 300 fb^{-1} for leading lepton $p_T^{\ell_1}$ (left), dilepton mass $m_{\ell\ell}$ (center) and opening angle $|\Delta\phi_{\ell\ell}|$ (right). Electron-muon preselection $p_T^{e(\mu)} > 18(15) \text{ GeV}$, $|\eta_\ell| < 2.5$, and vertex isolation $\Delta z_{\min} > 1 \text{ mm}$ via $(\varepsilon_{\text{PU}}, \varepsilon_{\text{UE}}) = (50\%, 0.4\%)$ are applied. SM (BSM) elastic $\gamma\gamma \rightarrow \tau\tau$ is the solid (dashed) line; other processes are stacked histograms.

limit of ideal detector efficiency and resolution. Quark-induced ditau $qq \rightarrow \tau\tau \rightarrow e\nu\nu\mu\nu$ (Drell-Yan) and diboson $qq \rightarrow WW \rightarrow e\nu\mu\nu$ dominate reducible backgrounds; photon-induced diboson $\gamma\gamma \rightarrow WW \rightarrow e\nu\mu\nu$ dominates irreducible backgrounds. We design an (i) *observation analysis* optimized for extracting the SM $\gamma\gamma \rightarrow \tau\tau$ signal from backgrounds and (ii) *dipole analysis* targeting BSM deviations amid backgrounds.

To reject reducible quark-induced backgrounds, we apply the track-vertex isolation technique [90, 91]. This requires the electron-muon principal vertex (PV) and track nearest to the PV have longitudinal separation $\Delta z_{\min} = |z_{\text{trk}}^{\min} - z_{\text{PV}}|$ (Fig. 1, right). This isolation (track veto) condition selects photon-fusion processes that exhibit no additional tracks associated to the PV, whereas quark-induced backgrounds have many tracks from underlying event (UE) in proton breakup. We follow Ref. [92] and emulate the $\Delta z_{\min} > 1 \text{ mm}$ condition assuming nominal $p_T^{\text{trk}} > 500 \text{ MeV}$ by applying a $\varepsilon_{\text{UE}} = 0.4\%$ efficiency to our quark-induced MC ($qq \rightarrow WW, \tau\tau$). Pileup tracks can also accidentally fall within the veto window, so we further apply a $\varepsilon_{\text{PU}} = 50\%$ efficiency based on data [91, 92] to all MC, which depends on the process-independent track density governed by the beamspot width $\sigma_z^{\text{beam}} \simeq 38 \text{ mm}$ in Run 2 [91]. We consider $\varepsilon_{\text{UE}} = 0.4\%$ as conservative given measurements show this is nearer 0.1% in $Z \rightarrow ee/\mu\mu$ data [91]; the difference arises from UE mismodelling in simulation [152]. We normalize our single (double) dissociative MADGRAPH MC to 0.5 (0.1) of the elastic cross-section to account for vertex isolation and soft survival based on Ref. [153]. Reconstructing UE tracks outside nominal acceptance would improve ε_{UE} by (i) increasing tracker acceptance $|\eta^{\text{trk}}| < 4$ at HL-LHC and (ii) reducing track thresholds to $p_T^{\text{trk}} > 200 \text{ MeV}$. A $p_T^{\text{trk}} > 100 \text{ MeV}$ threshold is feasible [154], but practically achieving this requires $p_T^{\text{trk}} > 200 \text{ MeV}$ to control fake tracks [155]. Low- p_T tracking requires unconventional data processing that reconstructs a subset of events passing kinematic selection offline rather than all events online, akin to ATLAS *de-*

layed stream and CMS *data parking* paradigms. We use a simple $\varepsilon_{\text{UE}} = 0.04\%$ benchmark to capture these possible improvements. Increased $p_T^{\text{trk}} > 1 \text{ GeV}$ [92] and pileup nuance HL-LHC extrapolations beyond the scope of this work, so we capture this simply with $\varepsilon_{\text{PU}} = 10\%$. These considerations motivate the $\varepsilon_{\text{UE}} \in [0.4\%, 0.04\%]$ and $\varepsilon_{\text{PU}} \in [50\%, 10\%]$ benchmarks in our projections.

Turning to electron-muon kinematics, we henceforth denote $\ell \in [e, \mu]$. The electron-muon pair from $\gamma\gamma \rightarrow \tau\tau$ is nearly back-to-back, so requiring the azimuthal opening angle satisfy $|\Delta\phi_{\ell\ell}| > 3.1$ provides 77% signal efficiency with little BSM dependence for 14% $qq \rightarrow \tau\tau$ and 3% WW efficiency. While the dilepton invariant mass $m_{\ell\ell}$ from $qq \rightarrow \tau\tau$ peaks around 40 GeV from resonant Z -boson production, a looser requirement $m_{\ell\ell} > 20 \text{ GeV}$ retains greater signal efficiency. Figure 3 shows $p_T^{\ell_1}$, $m_{\ell\ell}$, $|\Delta\phi_{\ell\ell}|$ distributions motivating the selection. We also require the stransverse mass defined in Refs. [125, 156, 157] satisfy $m_{\text{T}2}^{100} < 101 \text{ GeV}$, which is bounded from above by an endpoint at m_τ for $\tau\tau \rightarrow e\nu\nu\mu\nu$. Similar to Ref. [82], we use the dilepton $p_T^{\ell\ell}$ as the missing transverse momentum proxy in $m_{\text{T}2}^{100}$. To summarize the event selection:

- *Observation analysis* considers both elastic and dissociative $\gamma\gamma \rightarrow \tau\tau$ as signal following Refs. [91, 92], applying $p_T^{e(\mu)} > 18(15) \text{ GeV}$, $|\eta_\ell| < 2.5$, $m_{\ell\ell} > 20 \text{ GeV}$, $\Delta z_{\min} > 1 \text{ mm}$ (via $\varepsilon_{\text{UE}}, \varepsilon_{\text{PU}}$), $|\Delta\phi_{\ell\ell}| > 3.1$, $m_{\text{T}2}^{100} < 101 \text{ GeV}$.
- *Dipole analysis* exploits the harder BSM p_T^{ℓ} spectrum by binning in leading lepton $p_T^{e_1(\mu_1)} \in [18(15), 40, \infty]$, introduced in Ref. [49], subtracting dissociative $\gamma\gamma \rightarrow \tau\tau$ to leave only elastic $\gamma\gamma \rightarrow \tau\tau$ as signal. We use two bins for simplicity, but future work could improve sensitivity via finer binning.

For systematic uncertainties, we outline strategies for experimentalists to control them with powerful data-driven techniques. The dominant background systematic is UE track modelling, where control samples of Drell-Yan $qq \rightarrow \ell\ell$ can constrain $qq \rightarrow \tau\tau$ to percent-level

accuracy [90, 91]. The dominant $\gamma\gamma \rightarrow \tau\tau$ signal uncertainties arise from initial-state dynamics that we could estimate to be $\mathcal{O}(10\%)$ by comparing photon fluxes (Appendix 2) or alternative generators [153, 158, 159]. Fortunately, we can constrain these by measuring the high-statistics standard-candle $\gamma\gamma \rightarrow \ell\ell$ process (24 pb with $p_T^\ell > 5$ GeV, 3.6×10^6 events at 300 fb^{-1}) to correct both absolute $\gamma\gamma \rightarrow \tau\tau$ cross-sections and generator-level kinematics important for dipole shape analyses. Deriving such corrections from $\gamma\gamma \rightarrow ee/\mu\mu$ for $\gamma\gamma \rightarrow \tau\tau$ is well justified given the flavor independence of both initial-state proton soft-survival physics and QED final-state radiation. ATLAS has deployed these control techniques in similar measurements [25, 91]. We emphasize measuring dilepton mass $m_{\ell\ell}$ and rapidity $y_{\ell\ell}$ in distinct azimuthal angle $|\Delta\phi_{\ell\ell}|$ regions (or the correlated $p_T^{\ell\ell}$) would probe the composition of dissociative $pp \rightarrow p(\gamma\gamma \rightarrow \ell\ell)p^*$ enhanced at low $|\Delta\phi_{\ell\ell}| < 3.1$. This ensures simulation can accurately model and subtract dissociative production so only the elastic $\gamma\gamma \rightarrow \tau\tau$ signal remains for measuring EM dipoles in the $q_\gamma^2 \rightarrow 0$ limit. From recent $\gamma\gamma \rightarrow \ell\ell$ measurements [60, 90], we anticipate such data-driven corrections to $\gamma\gamma \rightarrow \tau\tau$ predictions can reach percent-level accuracy. With HL-LHC statistics, we anticipate experimental systematics to be limiting: luminosity uncertainties already reach 0.8% precision [160], while electron/muon momentum calibration will limit kinematic corrections, where the ee channel and upgraded trackers will enable tuning in $2.5 < |\eta_e| < 4$. Together, this motivates the assumed [1% 5%] systematics for benchmarking our projections, similar to the approach of Ref. [92].

IV. SENSITIVITY PROJECTIONS

Applying the event selection and assuming 300 fb^{-1} luminosity, we find our *observation analysis* yields $S = 121$ signal and $B = 443$ background counts ($S/B = 0.27$) assuming $(\varepsilon_{\text{UE}}, \varepsilon_{\text{PU}}) = (0.4\%, 50\%)$. Quark-induced processes $qq \rightarrow \tau\tau$ (96%) and $qq \rightarrow WW$ (3%) dominate the background composition with $\gamma\gamma \rightarrow WW$ in remainder. Evaluating the Poissonian asymptotic significance $Z_A(S, B, \zeta_b)$ [161, 162] assuming ζ_b background systematics, this exceeds five standard deviations $Z_A = 5.4$ for $\zeta_b = 1\%$. Assuming the more accurate value of $\varepsilon_{\text{UE}} = 0.1\%$, $Z_A = 8.5$ is feasible for $\zeta_b = 5\%$. This establishes a procedure to observe $\gamma\gamma \rightarrow \tau\tau$ using standard pp runs and tracking.

We estimate our *dipole analysis* sensitivity to BSM δa_τ using a χ^2 statistical test against the SM null hypothesis

$$\chi_r^2 = \frac{(S_{\text{SM+BSM}} - S_{\text{SM}})^2}{\sigma_{\text{stat}}^2 + \sigma_{\text{syst}}^2}. \quad (6)$$

We evaluate region r with B background yield, S_{SM} ($S_{\text{SM+BSM}}$) signal yield assuming SM (nonzero δa_τ) couplings, statistical $\sigma_{\text{stat}}^2 = B + S_{\text{SM+BSM}}$ and systematic $\sigma_{\text{syst}}^2 = (\zeta_b B)^2 + (\zeta_s S_{\text{SM+BSM}})^2$ uncertainties parameterized by $\zeta_{b,s}$. We consider a simplified scheme that as-

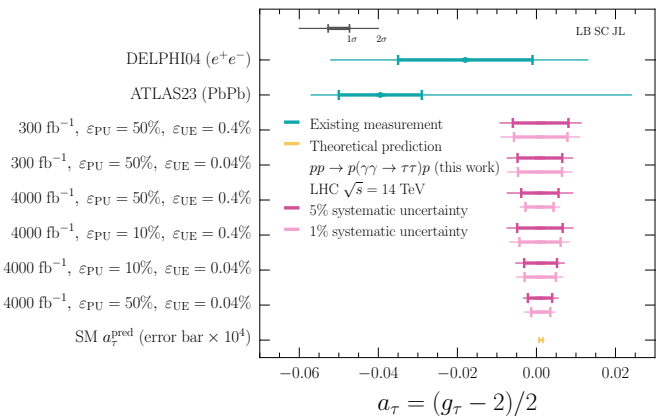


FIG. 4. Summary of tau-lepton magnetic dipole $a_\tau = (g_\tau - 2)/2$ sensitivity. Our projections (pink) assume 300 fb^{-1} and 4000 fb^{-1} luminosities for various pileup ε_{PU} and underlying-event ε_{UE} efficiencies with 5% (dark) and 1% (light) systematics. Displayed are existing DELPHI [22] and ATLAS [25] constraints (blue) alongside the SM prediction a_τ^{pred} (orange) [27]. The thick (thin) lines indicate 68% CL (95% CL) limits.

sumes $\zeta = \zeta_s = \zeta_b$ for the benchmarks $\zeta \in [1\%, 5\%]$ and are uncorrelated to statistically combine using $\chi^2 = \sum_r \chi_r^2$. The inequality $\chi^2 < 1$ ($\chi^2 < 3.84$) defines the 68% CL (95% CL) constraints on δa_τ .

Figure 4 summarizes our projected sensitivity for $a_\tau = a_\tau^{\text{SM}} + \delta a_\tau$. With 300 fb^{-1} luminosity, we find $-0.0092 < a_\tau < 0.011$ at 95% CL for the benchmarks $(\zeta, \varepsilon_{\text{PU}}, \varepsilon_{\text{UE}}) = (5\%, 50\%, 0.4\%)$. This is a four-fold improvement in magnitude over existing LEP [22–24] and LHC [25, 26] limits. Setting $C_{\tau B} = -1$ as a benchmark in Eq. (3), this corresponds to new physics scale sensitivity reaching $\Lambda_{C=-1}^{95} > 430$ GeV at 95% CL (from $\Lambda_{C=-1}^{95} > 190$ GeV at LEP). For 4000 fb^{-1} HL-LHC extrapolation, we also loosen $p_T^\ell > 10$ GeV, $|\eta_e| < 4$ GeV [163] to find an eightfold improvement beyond LEP $-0.0029 < a_\tau < 0.0046$ for the most optimistic scenario $(\zeta, \varepsilon_{\text{PU}}, \varepsilon_{\text{UE}}) = (1\%, 50\%, 0.04\%)$, corresponding to $\Lambda_{C=-1}^{95} > 680$ GeV. This HL-LHC reach degrades modestly to $-0.0067 < a_\tau < 0.0082$ with more realistic benchmarks $(\zeta, \varepsilon_{\text{PU}}, \varepsilon_{\text{UE}}) = (1\%, 10\%, 0.4\%)$. Our results establish an important strategy to overcome the longstanding obstacles of measuring $\gamma\gamma \rightarrow \tau\tau$ and a_τ in standard LHC runs. This introduces a novel avenue toward BSM physics via precision competitive with the landmark one-loop QED prediction $\alpha_{\text{EM}}/2\pi \simeq 0.0012$.

In summary, we proposed the strategy to measure $\gamma\gamma \rightarrow \tau\tau$ in LHC proton beams, with $-0.0092 < a_\tau < 0.011$ (95% CL) dipole sensitivity assuming 300 fb^{-1} luminosity and 5% systematics. This opens future work to develop triggers and track-veto strategies for hadronic channels, machine learning optimization, CP-sensitive observables for electric dipoles, and combinations with ALICE, LHCb, and heavy ions. Experimental realization would furnish a novel precision tau-lepton dipole program that could reveal new physics in quantum fluctuations.

ACKNOWLEDGMENTS

We thank Will Barter, Markus Diehl, Aleksandra Dimitrievska, Mateusz Dyndal, Zahra Ghorbanimoghaddam, Lucian Harland-Lang, Oldrich Kepka, Jakub Kremer, Valerie Lang, Kristin Lohwasser, Maeve Madigan, Klaus Mönig, Anna Mullin, Simone Pagan Griso, Andrew Pilkington, Philip Sommer, and Weronika Stanek-Maslouska for helpful discussions. We are grateful to the hospi-

tality of the Institute for Particle Physics Phenomenology at Durham University hosting the *Photon-induced Processes Workshop*, and University of Hamburg hosting the *European Physical Society Conference on High Energy Physics*, which facilitated in-person collaboration. LB and SC are supported by the Helmholtz Association “Young Investigator Group” initiative. JL is supported by a Junior Research Fellowship at Trinity College, University of Cambridge.

-
- * lydia.beresford@desy.de
 † savannah.clawson@desy.de
 ‡ jesseliu@hep.phy.cam.ac.uk
- [1] J. S. Schwinger, “On Quantum-Electrodynamics and the Magnetic Moment of the Electron,” *Phys. Rev.* **73**, 416–417 (1948).
 [2] P. Kusch and H. M. Foley, “The Magnetic Moment of the Electron,” *Phys. Rev.* **74**, 250 (1948).
 [3] B. Odom, D. Hanneke, B. D’Urso, and G. Gabrielse, “New Measurement of the Electron Magnetic Moment Using a One-Electron Quantum Cyclotron,” *Phys. Rev. Lett.* **97**, 030801 (2006).
 [4] D. Hanneke, S. Fogwell Hoogerheide, and G. Gabrielse, “Cavity Control of a Single-Electron Quantum Cyclotron: Measuring the Electron Magnetic Moment,” *Phys. Rev. A* **83**, 052122 (2011), arXiv:1009.4831 [physics.atom-ph].
 [5] R. Bouchendira, P. Cladé, S. Guellati-Khélifa, F. Nez, and F. Biraben, “New Determination of the Fine Structure Constant and Test of the Quantum Electrodynamics,” *Phys. Rev. Lett.* **106**, 080801 (2011).
 [6] T. Aoyama, M. Hayakawa, T. Kinoshita, and M. Nio, “Tenth-Order QED Contribution to the Electron $g-2$ and an Improved Value of the Fine Structure Constant,” *Phys. Rev. Lett.* **109**, 111807 (2012), arXiv:1205.5368 [hep-ph].
 [7] R. H. Parker, C. Yu, W. Zhong, B. Estey, and H. Müller, “Measurement of the fine-structure constant as a test of the Standard Model,” *Science* **360**, 191–195 (2018).
 [8] T. Aoyama, M. Hayakawa, T. Kinoshita, and M. Nio, “Complete Tenth-Order QED Contribution to the Muon $g-2$,” *Phys. Rev. Lett.* **109**, 111808 (2012), arXiv:1205.5370 [hep-ph].
 [9] A. Keshavarzi, D. Nomura, and T. Teubner, “Muon $g - 2$ and $\alpha(M_Z^2)$: a new data-based analysis,” *Phys. Rev. D* **97**, 114025 (2018), arXiv:1802.02995 [hep-ph].
 [10] M. Davier, A. Hoecker, B. Malaescu, and Z. Zhang, “A new evaluation of the hadronic vacuum polarisation contributions to the muon anomalous magnetic moment and to $\alpha(m_Z^2)$,” *Eur. Phys. J. C* **80**, 241 (2020), arXiv:1908.00921 [hep-ph].
 [11] L. Morel, Z. Yao, P. Cladé, and S. Guellati-Khélifa, “Determination of the fine-structure constant with an accuracy of 81 parts per trillion,” *Nature* **588**, 61–65 (2020).
 [12] X. Fan, T. G. Myers, B. A. D. Sukra, and G. Gabrielse, “Measurement of the Electron Magnetic Moment,” *Phys. Rev. Lett.* **130**, 071801 (2023), arXiv:2209.13084 [physics.atom-ph].
 [13] G. W. Bennett *et al.* (Muon $g-2$), “Final Report of the Muon E821 Anomalous Magnetic Moment Measurement at BNL,” *Phys. Rev. D* **73**, 072003 (2006), arXiv:hep-ex/0602035 [hep-ex].
 [14] B. Abi *et al.* (Muon $g - 2$), “Measurement of the Positive Muon Anomalous Magnetic Moment to 0.46 ppm,” *Phys. Rev. Lett.* **126**, 141801 (2021), arXiv:2104.03281 [hep-ex].
 [15] D. P. Aguillard *et al.* (Muon $g - 2$), “Measurement of the Positive Muon Anomalous Magnetic Moment to 0.20 ppm,” *Phys. Rev. Lett.* **131**, 161802 (2023), arXiv:2308.06230 [hep-ex].
 [16] T. Aoyama *et al.*, “The anomalous magnetic moment of the muon in the Standard Model,” *Phys. Rept.* **887**, 1–166 (2020), arXiv:2006.04822 [hep-ph].
 [17] M. Tanabashi *et al.* (Particle Data Group), “Review of Particle Physics,” *Phys. Rev. D* **98**, 030001 (2018).
 [18] ALEPH Collaboration, “Updated measurement of the tau lepton lifetime,” *Phys. Lett. B* **414**, 362–372 (1997), arXiv:hep-ex/9710026.
 [19] DELPHI Collaboration, “A Precise measurement of the tau lifetime,” *Eur. Phys. J. C* **36**, 283–296 (2004), arXiv:hep-ex/0410010.
 [20] L3 Collaboration, “Measurement of the lifetime of the τ lepton,” *Phys. Lett. B* **479**, 67–78 (2000), arXiv:hep-ex/0003023.
 [21] Belle Collaboration, “Measurement of the τ -lepton lifetime at Belle,” *Phys. Rev. Lett.* **112**, 031801 (2014), arXiv:1310.8503 [hep-ex].
 [22] DELPHI Collaboration, “Study of tau-pair production in photon-photon collisions at LEP and limits on the anomalous electromagnetic moments of the tau lepton,” *Eur. Phys. J. C* **35**, 159–170 (2004), arXiv:hep-ex/0406010 [hep-ex].
 [23] L3 Collaboration, “Measurement of the anomalous magnetic and electric dipole moments of the tau lepton,” *Phys. Lett. B* **434**, 169–179 (1998).
 [24] OPAL Collaboration, “An Upper limit on the anomalous magnetic moment of the tau lepton,” *Phys. Lett. B* **431**, 188–198 (1998), arXiv:hep-ex/9803020 [hep-ex].
 [25] ATLAS Collaboration, “Observation of the $\gamma\gamma \rightarrow \tau\tau$ Process in Pb + Pb Collisions and Constraints on the τ -Lepton Anomalous Magnetic Moment with the ATLAS Detector,” *Phys. Rev. Lett.* **131**, 151802 (2023), arXiv:2204.13478 [hep-ex].
 [26] CMS Collaboration, “Observation of τ Lepton Pair Production in Ultraperipheral Pb-Pb Collisions at $\sqrt{s_{NN}} = 5.02$ TeV,” *Phys. Rev. Lett.* **131**, 151803 (2023),

- arXiv:2206.05192 [nucl-ex].
- [27] S. Eidelman and M. Passera, “Theory of the tau lepton anomalous magnetic moment,” *Mod. Phys. Lett. A* **22**, 159–179 (2007), arXiv:hep-ph/0701260 [hep-ph].
- [28] T. Fukuyama, A. Ilakovac, and T. Kikuchi, “Lepton flavor violating leptonic/semileptonic decays of charged leptons in the minimal supersymmetric standard model,” *Eur. Phys. J. C* **56**, 125–146 (2008), arXiv:hep-ph/0506295 [hep-ph].
- [29] B. Dutta and Y. Mimura, “Electron $g - 2$ with flavor violation in MSSM,” *Phys. Lett. B* **790**, 563–567 (2019), arXiv:1811.10209 [hep-ph].
- [30] H. Davoudiasl and W. J. Marciano, “Tale of two anomalies,” *Phys. Rev. D* **98**, 075011 (2018), arXiv:1806.10252 [hep-ph].
- [31] M. Bauer, M. Neubert, S. Renner, M. Schnubel, and A. Thamm, “Axionlike Particles, Lepton-Flavor Violation, and a New Explanation of a_μ and a_e ,” *Phys. Rev. Lett.* **124**, 211803 (2020), arXiv:1908.00008 [hep-ph].
- [32] M. Endo and W. Yin, “Explaining electron and muon $g - 2$ anomaly in SUSY without lepton-flavor mixings,” *JHEP* **08**, 122 (2019), arXiv:1906.08768 [hep-ph].
- [33] LHCb Collaboration, “Measurement of the ratio of branching fractions $\mathcal{B}(\bar{B}^0 \rightarrow D^{*+}\tau^-\bar{\nu}_\tau)/\mathcal{B}(\bar{B}^0 \rightarrow D^{*+}\mu^-\bar{\nu}_\mu)$,” *Phys. Rev. Lett.* **115**, 111803 (2015), [Erratum: *Phys. Rev. Lett.* **115** (2015) 159901], arXiv:1506.08614 [hep-ex].
- [34] LHCb Collaboration, “Measurement of the ratios of branching fractions $\mathcal{R}(D^*)$ and $\mathcal{R}(D^0)$,” *Phys. Rev. Lett.* **131**, 111802 (2023), arXiv:2302.02886 [hep-ex].
- [35] Belle Collaboration, “Measurement of $\mathcal{R}(D)$ and $\mathcal{R}(D^*)$ with a semilepton tagging method,” (2019), arXiv:1904.08794 [hep-ex].
- [36] B. Allanach, F. S. Queiroz, A. Strumia, and S. Sun, “ Z' models for the LHCb and $g - 2$ muon anomalies,” *Phys. Rev. D* **93**, 055045 (2016), [Erratum: *Phys. Rev. D* **95** (2017) 119902], arXiv:1511.07447 [hep-ph].
- [37] S. Di Chiara, A. Fowlie, S. Fraser, C. Marzo, L. Marzola, M. Raidal, and C. Spethmann, “Minimal flavor-changing Z' models and muon $g - 2$ after the R_{K^*} measurement,” *Nucl. Phys. B* **923**, 245–257 (2017), arXiv:1704.06200 [hep-ph].
- [38] A. Biswas and A. Shaw, “Reconciling dark matter, $R_{K^{(*)}}$ anomalies and $(g - 2)_\mu$ in an $L_\mu - L_\tau$ scenario,” *JHEP* **05**, 165 (2019), arXiv:1903.08745 [hep-ph].
- [39] W. Yin and N. Yokozaki, “Splitting mass spectra and muon $g - 2$ in Higgs-anomaly mediation,” *Phys. Lett. B* **762**, 72–79 (2016), arXiv:1607.05705 [hep-ph].
- [40] M. Yamaguchi and W. Yin, “A novel approach to finely tuned supersymmetric standard models: The case of the non-universal Higgs mass model,” *PTEP* **2018**, 023B06 (2018), arXiv:1606.04953 [hep-ph].
- [41] K. S. Babu, T. Fukuyama, S. Khan, and S. Saad, “Peccei-Quinn Symmetry and Nucleon Decay in Renormalizable SUSY $SO(10)$,” *JHEP* **06**, 045 (2019), arXiv:1812.11695 [hep-ph].
- [42] S. Iguro and T. Kitahara, “Electric Dipole Moments as Probes of B Anomaly,” (2023), arXiv:2307.11751 [hep-ph].
- [43] B. Allanach and J. Davighi, “The Rumble in the Meson: a leptoquark versus a Z' to fit $b \rightarrow s\mu^+\mu^-$ anomalies including 2022 LHCb $R_{K^{(*)}}$ measurements,” *JHEP* **04**, 033 (2023), arXiv:2211.11766 [hep-ph].
- [44] B. Allanach and A. Mullin, “Plan B: New Z' models for $b \rightarrow sl^+l^-$ anomalies,” *JHEP* **09**, 173 (2023), arXiv:2306.08669 [hep-ph].
- [45] T. Moroi, “The Muon anomalous magnetic dipole moment in the minimal supersymmetric standard model,” *Phys. Rev. D* **53**, 6565–6575 (1996), [Erratum: *Phys. Rev. D* **56**, 4424 (1997)], arXiv:hep-ph/9512396.
- [46] T. Ibrahim and P. Nath, “CP violation and the muon anomaly in $N=1$ supergravity,” *Phys. Rev. D* **61**, 095008 (2000), arXiv:hep-ph/9907555.
- [47] S. P. Martin and J. D. Wells, “Muon Anomalous Magnetic Dipole Moment in Supersymmetric Theories,” *Phys. Rev. D* **64**, 035003 (2001), arXiv:hep-ph/0103067 [hep-ph].
- [48] F. del Aguila, F. Cornet, and J. I. Illana, “The possibility of using a large heavy-ion collider for measuring the electromagnetic properties of the tau lepton,” *Phys. Lett. B* **271**, 256–260 (1991).
- [49] L. Beresford and J. Liu, “New physics and tau $g-2$ using LHC heavy ion collisions,” *Phys. Rev. D* **102**, 113008 (2020), [Erratum: *Phys. Rev. D* **106** (2022) 039902], arXiv:1908.05180 [hep-ph].
- [50] M. Dyndal, M. Klusek-Gawenda, M. Schott, and A. Szczurek, “Anomalous electromagnetic moments of τ lepton in $\gamma\gamma \rightarrow \tau^+\tau^-$ reaction in Pb+Pb collisions at the LHC,” *Phys. Lett. B* **809**, 135682 (2020), arXiv:2002.05503 [hep-ph].
- [51] N. Burmasov, E. Kryshen, P. Bühler, and R. Lavicka, “Feasibility Studies of Tau-Lepton Anomalous Magnetic Moment Measurements in Ultraperipheral Collisions at the LHC,” *Phys. Part. Nucl.* **54**, 590–594 (2023).
- [52] V. P. Goncalves, D. E. Martins, and M. S. Rangel, “Exclusive dilepton production at forward rapidities in $PbPb$ collisions,” *Eur. Phys. J. C* **81**, 220 (2021), arXiv:2012.08923 [hep-ph].
- [53] M. Verducci, N. Vignaroli, C. Roda, and V. Cavasinni, “A study of the measurement of the τ lepton anomalous magnetic moment in high energy lead-lead collisions at LHC,” (2023), arXiv:2307.15160 [hep-ph].
- [54] K. Piotrkowski, “Tagging two photon production at the CERN LHC,” *Phys. Rev. D* **63**, 071502 (2001), arXiv:hep-ex/0009065 [hep-ex].
- [55] A. J. Baltz, “The Physics of Ultraperipheral Collisions at the LHC,” *Phys. Rept.* **458**, 1–171 (2008), arXiv:0706.3356 [nucl-ex].
- [56] M. G. Albrow *et al.* (FP420 R & D), “The FP420 R & D Project: Higgs and New Physics with forward protons at the LHC,” *JINST* **4**, T10001 (2009), arXiv:0806.0302 [hep-ex].
- [57] J. de Favereau de Jeneret, V. Lemaitre, Y. Liu, S. Ovin, T. Pierzchala, K. Piotrkowski, X. Rouby, N. Schul, and M. Vander Donckt, “High energy photon interactions at the LHC,” (2009), arXiv:0908.2020 [hep-ph].
- [58] D. d’Enterria and J.-P. Lansberg, “Study of Higgs boson production and its $b\bar{b}$ decay in $\gamma-\gamma$ processes in proton-nucleus collisions at the LHC,” *Phys. Rev. D* **81**, 014004 (2010), arXiv:0909.3047 [hep-ph].
- [59] ATLAS Collaboration, “Measurement of exclusive $\gamma\gamma \rightarrow \ell^+\ell^-$ production in proton-proton collisions at $\sqrt{s} = 7$ TeV with the ATLAS detector,” *Phys. Lett. B* **749**, 242–261 (2015), arXiv:1506.07098 [hep-ex].
- [60] ATLAS Collaboration, “Measurement of the exclusive $\gamma\gamma \rightarrow \mu^+\mu^-$ process in proton-proton collisions at $\sqrt{s} = 13$ TeV with the ATLAS detector,” *Phys. Lett. B* **777**, 303–323 (2018), arXiv:1708.04053 [hep-ex].

- [61] ATLAS Collaboration, “Measurement of exclusive $\gamma\gamma \rightarrow W^+W^-$ production and search for exclusive Higgs boson production in pp collisions at $\sqrt{s} = 8$ TeV using the ATLAS detector,” *Phys. Rev. D* **94**, 032011 (2016), [arXiv:1607.03745 \[hep-ex\]](#).
- [62] CMS Collaboration, “Search for exclusive or semi-exclusive photon pair production and observation of exclusive and semi-exclusive electron pair production in pp collisions at $\sqrt{s} = 7$ TeV,” *JHEP* **11**, 080 (2012), [arXiv:1209.1666 \[hep-ex\]](#).
- [63] CMS Collaboration, “Study of Exclusive Two-Photon Production of W^+W^- in pp Collisions at $\sqrt{s} = 7$ TeV and Constraints on Anomalous Quartic Gauge Couplings,” *JHEP* **07**, 116 (2013), [arXiv:1305.5596 \[hep-ex\]](#).
- [64] CMS Collaboration, “Evidence for exclusive $\gamma\gamma \rightarrow W^+W^-$ production and constraints on anomalous quartic gauge couplings in pp collisions at $\sqrt{s} = 7$ and 8 TeV,” *JHEP* **08**, 119 (2016), [arXiv:1604.04464 \[hep-ex\]](#).
- [65] ATLAS Collaboration, “Measurement of light-by-light scattering and search for axion-like particles with 2.2 nb^{-1} of Pb+Pb data with the ATLAS detector,” *JHEP* **03**, 243 (2021), [Erratum: *JHEP* **11** (2021) 050], [arXiv:2008.05355 \[hep-ex\]](#).
- [66] ATLAS Collaboration, “Exclusive dimuon production in ultraperipheral Pb+Pb collisions at $\sqrt{s_{NN}} = 5.02$ TeV with ATLAS,” *Phys. Rev. C* **104**, 024906 (2021), [arXiv:2011.12211 \[nucl-ex\]](#).
- [67] ATLAS Collaboration, “Exclusive dielectron production in ultraperipheral Pb+Pb collisions at $\sqrt{s_{NN}} = 5.02$ TeV with ATLAS,” *JHEP* **06**, 182 (2023), [arXiv:2207.12781 \[nucl-ex\]](#).
- [68] D. d’Enterria and G. G. da Silveira, “Observing light-by-light scattering at the Large Hadron Collider,” *Phys. Rev. Lett.* **111**, 080405 (2013), [Erratum: *Phys. Rev. Lett.* **116** (2016) 129901], [arXiv:1305.7142 \[hep-ph\]](#).
- [69] ATLAS Collaboration, “Evidence for light-by-light scattering in heavy-ion collisions with the ATLAS detector at the LHC,” *Nat. Phys.* **13**, 852–858 (2017), [arXiv:1702.01625 \[hep-ex\]](#).
- [70] CMS Collaboration, “Evidence for light-by-light scattering and searches for axion-like particles in ultraperipheral PbPb collisions at $\sqrt{s_{NN}} = 5.02$ TeV,” *Phys. Lett. B* **797**, 134826 (2019), [arXiv:1810.04602 \[hep-ex\]](#).
- [71] ATLAS Collaboration, “Observation of light-by-light scattering in ultraperipheral Pb+Pb collisions with the ATLAS detector,” *Phys. Rev. Lett.* **123**, 052001 (2019), [arXiv:1904.03536 \[hep-ex\]](#).
- [72] J. Howarth, “Elastic Potential: A proposal to discover elastic production of top quarks at the Large Hadron Collider,” (2020), [arXiv:2008.04249 \[hep-ph\]](#).
- [73] V. P. Gonçalves, D. E. Martins, M. S. Rangel, and M. Tasevsky, “Top quark pair production in the exclusive processes at the LHC,” *Phys. Rev. D* **102**, 074014 (2020), [arXiv:2007.04565 \[hep-ph\]](#).
- [74] E. Chapon, C. Royon, and O. Kepka, “Anomalous quartic $WW\gamma\gamma$, $ZZ\gamma\gamma$, and trilinear $WW\gamma$ couplings in two-photon processes at high luminosity at the LHC,” *Phys. Rev. D* **81**, 074003 (2010), [arXiv:0912.5161 \[hep-ph\]](#).
- [75] S. Fichet, G. von Gersdorff, O. Kepka, B. Lenzi, C. Royon, and M. Saimpert, “Probing new physics in diphoton production with proton tagging at the Large Hadron Collider,” *Phys. Rev. D* **89**, 114004 (2014), [arXiv:1312.5153 \[hep-ph\]](#).
- [76] J. Ellis, N. E. Mavromatos, and T. You, “Light-by-Light Scattering Constraint on Born-Infeld Theory,” *Phys. Rev. Lett.* **118**, 261802 (2017), [arXiv:1703.08450 \[hep-ph\]](#).
- [77] S. Knapen, T. Lin, H. K. Lou, and T. Melia, “Searching for Axionlike Particles with Ultraperipheral Heavy-Ion Collisions,” *Phys. Rev. Lett.* **118**, 171801 (2017), [arXiv:1607.06083 \[hep-ph\]](#).
- [78] C. Baldenegro, S. Fichet, G. von Gersdorff, and C. Royon, “Searching for axion-like particles with proton tagging at the LHC,” *JHEP* **06**, 131 (2018), [arXiv:1803.10835 \[hep-ph\]](#).
- [79] J. Ohnemus, T. F. Walsh, and P. M. Zerwas, “ $\gamma\gamma$ production of nonstrongly interacting SUSY particles at hadron colliders,” *Phys. Lett. B* **328**, 369–373 (1994), [arXiv:hep-ph/9402302 \[hep-ph\]](#).
- [80] N. Schul and K. Piotrkowski, “Detection of two-photon exclusive production of supersymmetric pairs at the LHC,” *Nucl. Phys. Proc. Suppl.* **179–180**, 289–297 (2008), [arXiv:0806.1097 \[hep-ph\]](#).
- [81] L. A. Harland-Lang, C. H. Kom, K. Sakurai, and W. J. Stirling, “Measuring the masses of a pair of semi-invisibly decaying particles in central exclusive production with forward proton tagging,” *Eur. Phys. J. C* **72**, 1969 (2012), [arXiv:1110.4320 \[hep-ph\]](#).
- [82] L. Beresford and J. Liu, “Search Strategy for Sleptons and Dark Matter Using the LHC as a Photon Collider,” *Phys. Rev. Lett.* **123**, 141801 (2019), [arXiv:1811.06465 \[hep-ph\]](#).
- [83] L. A. Harland-Lang, V. A. Khoze, M. G. Ryskin, and M. Tasevsky, “LHC Searches for Dark Matter in Compressed Mass Scenarios: Challenges in the Forward Proton Mode,” *JHEP* **04**, 010 (2019), [arXiv:1812.04886 \[hep-ph\]](#).
- [84] R. Bruce *et al.*, “New physics searches with heavy-ion collisions at the CERN Large Hadron Collider,” *J. Phys. G* **47**, 060501 (2020), [arXiv:1812.07688 \[hep-ph\]](#).
- [85] D. d’Enterria, M. A. Tamliah, L. Schoeffel, H.-S. Shao, and Y. Tayalati, “Collider constraints on massive gravitons coupling to photons,” *Phys. Lett. B* **846**, 138237 (2023), [arXiv:2306.15558 \[hep-ph\]](#).
- [86] ATLAS Collaboration, “Search for an axion-like particle with forward proton scattering in association with photon pairs at ATLAS,” *JHEP* **07**, 234 (2023), [arXiv:2304.10953 \[hep-ex\]](#).
- [87] CMS and TOTEM Collaborations, “First Search for Exclusive Diphoton Production at High Mass with Tagged Protons in Proton-Proton Collisions at $\sqrt{s} = 13$ TeV,” *Phys. Rev. Lett.* **129**, 011801 (2022), [arXiv:2110.05916 \[hep-ex\]](#).
- [88] CMS and TOTEM Collaborations, “Search for high-mass exclusive $\gamma\gamma \rightarrow WW$ and $\gamma\gamma \rightarrow ZZ$ production in proton-proton collisions at $\sqrt{s} = 13$ TeV,” *JHEP* **07**, 229 (2023), [arXiv:2211.16320 \[hep-ex\]](#).
- [89] S. Atag and A. A. Billur, “Possibility of Determining τ Lepton Electromagnetic Moments in $\gamma\gamma \rightarrow \tau^+\tau^-$ Process at the CERN-LHC,” *JHEP* **11**, 060 (2010), [arXiv:1005.2841 \[hep-ph\]](#).
- [90] ATLAS Collaboration, “Observation and Measurement of Forward Proton Scattering in Association with Lepton Pairs Produced via the Photon Fusion Mechanism at ATLAS,” *Phys. Rev. Lett.* **125**, 261801 (2020), [arXiv:2009.14537 \[hep-ex\]](#).
- [91] ATLAS Collaboration, “Observation of photon-induced

- W^+W^- production in pp collisions at $\sqrt{s} = 13$ TeV using the ATLAS detector,” *Phys. Lett. B* **816**, 136190 (2021), arXiv:2010.04019 [hep-ex].
- [92] ATLAS Collaboration, “Sensitivity to exclusive WW production in photon scattering at the High Luminosity LHC,” *ATL-PHYS-PUB-2021-026* (2021).
- [93] M. A. Samuel and G. Li, “How to measure the magnetic moment of the tau lepton,” *Int. J. Theor. Phys.* **33**, 1471–1477 (1994).
- [94] A. Hayreter and G. Valencia, “Constraining τ -lepton dipole moments and gluon couplings at the LHC,” *Phys. Rev. D* **88**, 013015 (2013), [Erratum: *Phys. Rev. D* 91 (2015) 099902], arXiv:1305.6833 [hep-ph].
- [95] I. Galon, A. Rajaraman, and T. M. P. Tait, “ $H \rightarrow \tau^+\tau^-\gamma$ as a probe of the τ magnetic dipole moment,” *JHEP* **12**, 111 (2016), arXiv:1610.01601 [hep-ph].
- [96] A. S. Fomin, A. Yu Korchin, A. Stocchi, S. Barsuk, and P. Robbe, “Feasibility of τ -lepton electromagnetic dipole moments measurement using bent crystal at the LHC,” *JHEP* **03**, 156 (2019), arXiv:1810.06699 [hep-ph].
- [97] J. Fu, M. A. Giorgi, L. Henry, D. Marangotto, F. Martínez Vidal, A. Merli, N. Neri, and J. Ruiz Vidal, “Novel Method for the Direct Measurement of the τ Lepton Dipole Moments,” *Phys. Rev. Lett.* **123**, 011801 (2019), arXiv:1901.04003 [hep-ex].
- [98] U. Haisch, L. Schnell, and J. Weiss, “LHC tau-pair production constraints on a_τ and d_τ ,” *SciPost Phys.* **16**, 048 (2024), arXiv:2307.14133 [hep-ph].
- [99] S. Eidelman, D. Epifanov, M. Fael, L. Mercolli, and M. Passera, “ τ dipole moments via radiative leptonic τ decays,” *JHEP* **03**, 140 (2016), arXiv:1601.07987 [hep-ph].
- [100] A. Crivellin, M. Hoferichter, and J. M. Roney, “Toward testing the magnetic moment of the tau at one part per million,” *Phys. Rev. D* **106**, 093007 (2022), arXiv:2111.10378 [hep-ph].
- [101] M. Köksal, A. A. Billur, A. Gutiérrez-Rodríguez, and M. A. Hernández-Ruíz, “Model-independent sensitivity estimates for the electromagnetic dipole moments of the τ -lepton at the CLIC,” *Phys. Rev. D* **98**, 015017 (2018), arXiv:1804.02373 [hep-ph].
- [102] A. A. Billur and M. Köksal, “Probe of the electromagnetic moments of the tau lepton in gamma-gamma collisions at the CLIC,” *Phys. Rev. D* **89**, 037301 (2014).
- [103] A. Rajaraman, J. N. Howard, R. Riley, and Tim M. P. Tait, “The τ Magnetic Dipole Moment at Future Lepton Colliders,” *LHEP* **2**, 5 (2019), arXiv:1810.09570 [hep-ph].
- [104] M. Köksal, “Search for the electromagnetic moments of the τ lepton in photon-photon collisions at the LHeC and the FCC-he,” *J. Phys. G* **46**, 065003 (2019), arXiv:1809.01963 [hep-ph].
- [105] A. Gutiérrez-Rodríguez, M. Köksal, A. A. Billur, and M. A. Hernández-Ruíz, “Feasibility at the LHC, FCC-he and CLIC for sensitivity estimates on anomalous τ -lepton couplings,” (2019), arXiv:1903.04135 [hep-ph].
- [106] J. J. Chwastowski, K. Piotrkowski, and M. Przybycien, “Exclusive lepton pair production at the electron-ion collider,” *Eur. Phys. J. C* **82**, 846 (2022), arXiv:2206.02466 [hep-ph].
- [107] M. Fael, L. Mercolli, and M. Passera, “Towards a determination of the tau lepton dipole moments,” *Nucl. Phys. Proc. Suppl.* **253-255**, 103–106 (2014), arXiv:1301.5302 [hep-ph].
- [108] M. Köksal, “Model-independent study on the anomalous $\tau\tau\gamma$ couplings at the ILC,” *Nucl. Phys. B* **971**, 115520 (2021), arXiv:2104.01003 [hep-ph].
- [109] X. Chen and Y. Wu, “Search for the Electric Dipole Moment and anomalous magnetic moment of the tau lepton at tau factories,” *JHEP* **10**, 089 (2019), arXiv:1803.00501 [hep-ph].
- [110] H. M. Tran and Y. Kurihara, “Tau $g-2$ at e^-e^+ colliders with momentum dependent form factor,” *Eur. Phys. J. C* **81**, 108 (2021), arXiv:2006.00660 [hep-ph].
- [111] M. Köksal, A. A. Billur, A. Gutiérrez-Rodríguez, and M. A. Hernández-Ruíz, “The $\mu^+\mu^-$ collider to sensitivity estimates on the magnetic and electric dipole moments of the tau-lepton,” *Int. J. Mod. Phys. A* **34**, 1950076 (2019), arXiv:1811.01188 [hep-ph].
- [112] S. Qian *et al.*, “Boosted Tau Lepton as a Microscope and Macroscope,” *Adv. High Energy Phys.* **2022**, 4931241 (2022), arXiv:2201.07808 [hep-ph].
- [113] ALEPH Collaboration, “Measurement of the tau polarization at LEP,” *Eur. Phys. J. C* **20**, 401–430 (2001), arXiv:hep-ex/0104038.
- [114] ATLAS Collaboration, “Measurement of τ polarisation in $Z/\gamma^* \rightarrow \tau\tau$ decays in proton-proton collisions at $\sqrt{s} = 8$ TeV with the ATLAS detector,” *Eur. Phys. J. C* **78**, 163 (2018), arXiv:1709.03490 [hep-ex].
- [115] CMS Collaboration, “Measurement of the τ lepton polarization in Z boson decays in proton-proton collisions at $\sqrt{s} = 13$ TeV,” *JHEP* **01**, 101 (2024), arXiv:2309.12408 [hep-ex].
- [116] ATLAS Collaboration, “Test of the universality of τ and μ lepton couplings in W -boson decays with the ATLAS detector,” *Nature Phys.* **17**, 813–818 (2021), arXiv:2007.14040 [hep-ex].
- [117] BaBar Collaboration, “Measurements of the τ mass and the mass difference of the τ^+ and τ^- at BABAR,” *Phys. Rev. D* **80**, 092005 (2009), arXiv:0909.3562 [hep-ex].
- [118] BESIII Collaboration, “Precision measurement of the mass of the τ lepton,” *Phys. Rev. D* **90**, 012001 (2014), arXiv:1405.1076 [hep-ex].
- [119] Belle-II Collaboration, “Measurement of the τ -lepton mass with the Belle II experiment,” *Phys. Rev. D* **108**, 032006 (2023), arXiv:2305.19116 [hep-ex].
- [120] D. Alves *et al.* (LHC New Physics Working Group), “Simplified Models for LHC New Physics Searches,” *J. Phys. G* **39**, 105005 (2012), arXiv:1105.2838 [hep-ph].
- [121] J. Abdallah *et al.*, “Simplified Models for Dark Matter Searches at the LHC,” *Phys. Dark Univ.* **9-10**, 8–23 (2015), arXiv:1506.03116 [hep-ph].
- [122] A. Barr and J. Liu, “Analysing parameter space correlations of recent 13 TeV gluino and squark searches in the pMSSM,” *Eur. Phys. J. C* **77**, 202 (2017), arXiv:1608.05379 [hep-ph].
- [123] ATLAS Collaboration, “Search for new phenomena in dijet mass and angular distributions from pp collisions at $\sqrt{s} = 13$ TeV with the ATLAS detector,” *Phys. Lett. B* **754**, 302–322 (2016), arXiv:1512.01530 [hep-ex].
- [124] ATLAS Collaboration, “Search for low-mass resonances decaying into two jets and produced in association with a photon using pp collisions at $\sqrt{s} = 13$ TeV with the ATLAS detector,” *Phys. Lett. B* **795**, 56–75 (2019), arXiv:1901.10917 [hep-ex].
- [125] ATLAS Collaboration, “Searches for electroweak production of supersymmetric particles with compressed

- mass spectra in $\sqrt{s} = 13$ TeV pp collisions with the ATLAS detector,” *Phys. Rev. D* **101**, 052005 (2020), arXiv:1911.12606 [hep-ex].
- [126] ATLAS Collaboration, “Search for direct stau production in events with two hadronic τ -leptons in $\sqrt{s} = 13$ TeV pp collisions with the ATLAS detector,” *Phys. Rev. D* **101**, 032009 (2020), arXiv:1911.06660 [hep-ex].
- [127] ATLAS Collaboration, “Search for heavy Higgs bosons decaying into two tau leptons with the ATLAS detector using pp collisions at $\sqrt{s} = 13$ TeV,” *Phys. Rev. Lett.* **125**, 051801 (2020), arXiv:2002.12223 [hep-ex].
- [128] CMS Collaboration, “Search for supersymmetric partners of electrons and muons in proton-proton collisions at $\sqrt{s} = 13$ TeV,” *Phys. Lett. B* **790**, 140–166 (2019), arXiv:1806.05264 [hep-ex].
- [129] CMS Collaboration, “Search for Supersymmetry with a Compressed Mass Spectrum in Events with a Soft τ Lepton, a Highly Energetic Jet, and Large Missing Transverse Momentum in Proton-Proton Collisions at $\sqrt{s} = 13$ TeV,” *Phys. Rev. Lett.* **124**, 041803 (2020), arXiv:1910.01185 [hep-ex].
- [130] CMS Collaboration, “Search for invisible decays of the Higgs boson produced via vector boson fusion in proton-proton collisions at $\sqrt{s} = 13$ TeV,” *Phys. Rev. D* **105**, 092007 (2022), arXiv:2201.11585 [hep-ex].
- [131] LHCb Collaboration, “Search for $A' \rightarrow \mu^+ \mu^-$ Decays,” *Phys. Rev. Lett.* **124**, 041801 (2020), arXiv:1910.06926 [hep-ex].
- [132] R. Escribano and E. Masso, “New bounds on the magnetic and electric moments of the tau lepton,” *Phys. Lett. B* **301**, 419–422 (1993).
- [133] B. Grzadkowski, M. Iskrzynski, M. Misiak, and J. Rosiek, “Dimension-Six Terms in the Standard Model Lagrangian,” *JHEP* **10**, 085 (2010), arXiv:1008.4884 [hep-ph].
- [134] A. Alloul, N. D. Christensen, C. Degrande, C. Duhr, and B. Fuks, “FeynRules 2.0 – A complete toolbox for tree-level phenomenology,” *Comput. Phys. Commun.* **185**, 2250–2300 (2014), arXiv:1310.1921 [hep-ph].
- [135] I. Brivio, Y. Jiang, and M. Trott, “The SMEFTsim package, theory and tools,” *JHEP* **12**, 070 (2017), arXiv:1709.06492 [hep-ph].
- [136] I. Brivio, “SMEFTsim 3.0 — a practical guide,” *JHEP* **04**, 073 (2021), arXiv:2012.11343 [hep-ph].
- [137] J. Alwall, M. Herquet, F. Maltoni, O. Mattelaer, and T. Stelzer, “MadGraph 5: Going Beyond,” *JHEP* **06**, 128 (2011), arXiv:1106.0522 [hep-ph].
- [138] J. Alwall *et al.*, “The automated computation of tree-level and next-to-leading order differential cross sections, and their matching to parton shower simulations,” *JHEP* **07**, 079 (2014), arXiv:1405.0301 [hep-ph].
- [139] V. M. Budnev, I. F. Ginzburg, G. V. Meledin, and V. G. Serbo, “The two photon particle production mechanism. Physical problems. Applications. Equivalent photon approximation,” *Phys. Rept.* **15**, 181–281 (1975).
- [140] H.-S. Shao and D. d’Enterria, “gamma-UPC: automated generation of exclusive photon-photon processes in ultraperipheral proton and nuclear collisions with varying form factors,” *JHEP* **09**, 248 (2022), arXiv:2207.03012 [hep-ph].
- [141] T. Sjostrand, S. Mrenna, and P. Z. Skands, “A Brief Introduction to PYTHIA 8.1,” *Comput. Phys. Commun.* **178**, 852–867 (2008), arXiv:0710.3820 [hep-ph].
- [142] C. Bierlich *et al.*, “A comprehensive guide to the physics and usage of PYTHIA 8.3,” *SciPost Phys. Codebases* **8** (2022), 10.21468/SciPostPhysCodeb.8, arXiv:2203.11601 [hep-ph].
- [143] “IPPP Workshop on the modeling of photon-induced processes,” (2023), <https://conference.ippp.dur.ac.uk/event/1193/>.
- [144] R. D. Ball *et al.*, “Parton distributions with LHC data,” *Nucl. Phys. B* **867**, 244–289 (2013), arXiv:1207.1303 [hep-ph].
- [145] M. L. Mangano, M. Moretti, F. Piccinini, and M. Trecani, “Matching matrix elements and shower evolution for top-quark production in hadronic collisions,” *JHEP* **01**, 013 (2007), arXiv:hep-ph/0611129 [hep-ph].
- [146] J. de Favereau, C. Delaere, P. Demin, A. Giammanco, V. Lemaitre, A. Mertens, and M. Selvaggi (DELPHES 3), “DELPHES 3, A modular framework for fast simulation of a generic collider experiment,” *JHEP* **02**, 057 (2014), arXiv:1307.6346 [hep-ex].
- [147] ATLAS Collaboration, “ATLAS Phase-II Upgrade Scoping Document,” (2015), 10.17181/CERN.7CRX.AJHP.
- [148] ATLAS Collaboration, “Performance of electron and photon triggers in ATLAS during LHC Run 2,” *Eur. Phys. J. C* **80**, 47 (2020), arXiv:1909.00761 [hep-ex].
- [149] ATLAS Collaboration, “Performance of the ATLAS muon triggers in Run 2,” *JINST* **15**, P09015 (2020), arXiv:2004.13447 [physics.ins-det].
- [150] ATLAS Collaboration, “Performance of the ATLAS Level-1 topological trigger in Run 2,” *Eur. Phys. J. C* **82**, 7 (2022), arXiv:2105.01416 [hep-ex].
- [151] ATLAS Collaboration, “Trigger menu in 2018,” *ATL-DQA-PUB-2019-001* (2019).
- [152] ATLAS Collaboration, “Measurement of distributions sensitive to the underlying event in inclusive Z -boson production in pp collisions at $\sqrt{s} = 13$ TeV with the ATLAS detector,” *Eur. Phys. J. C* **79**, 666 (2019), arXiv:1905.09752 [hep-ex].
- [153] L. A. Harland-Lang, M. Tasevsky, V. A. Khoze, and M. G. Ryskin, “A new approach to modelling elastic and inelastic photon-initiated production at the LHC: SuperChic 4,” *Eur. Phys. J. C* **80**, 925 (2020), arXiv:2007.12704 [hep-ph].
- [154] ATLAS Collaboration, “Charged-particle distributions at low transverse momentum in $\sqrt{s} = 13$ TeV pp interactions measured with the ATLAS detector at the LHC,” *Eur. Phys. J. C* **76**, 502 (2016), arXiv:1606.01133 [hep-ex].
- [155] W. P. McCormack *et al.* (ATLAS), “CTD2020: Minimum Pt Track Reconstruction in ATLAS,” *Proceedings of Connecting The Dots Workshop* (2020), 10.5281/zenodo.4088478.
- [156] A. Barr, C. Lester, and P. Stephens, “A variable for measuring masses at hadron colliders when missing energy is expected; m_{T2} : the truth behind the glamour,” *J. Phys. G* **29**, 2343–2363 (2003), arXiv:hep-ph/0304226 [hep-ph].
- [157] C. G. Lester and B. Nachman, “Bisection-based asymmetric M_{T2} computation: a higher precision calculator than existing symmetric methods,” *JHEP* **03**, 100 (2015), arXiv:1411.4312 [hep-ph].
- [158] L. A. Harland-Lang, V. A. Khoze, and M. G. Ryskin, “Exclusive LHC physics with heavy ions: SuperChic 3,” *Eur. Phys. J. C* **79**, 39 (2019), arXiv:1810.06567 [hep-ph].

- [159] L. A. Harland-Lang, A. D. Martin, R. Nathvani, and R. S. Thorne, “Ad Lucem: QED Parton Distribution Functions in the MMHT Framework,” *Eur. Phys. J. C* **79**, 811 (2019), arXiv:1907.02750 [hep-ph].
- [160] ATLAS Collaboration, “Luminosity determination in pp collisions at $\sqrt{s} = 13$ TeV using the ATLAS detector at the LHC,” *Eur. Phys. J. C* **83**, 982 (2023), arXiv:2212.09379 [hep-ex].
- [161] G. Cowan, “Discovery sensitivity for a counting experiment with background uncertainty,” Royal Holloway, London (2012), www.pp.rhul.ac.uk/~cowan/stat/medsig/medsigNote.pdf.
- [162] G. Cowan, K. Cranmer, E. Gross, and O. Vitells, “Asymptotic formulae for likelihood-based tests of new physics,” *Eur. Phys. J.* **C71**, 1554 (2011), [Erratum: *Eur. Phys. J.C* 73 (2013) 2501], arXiv:1007.1727 [physics.data-an].
- [163] ATLAS Collaboration, “Technical Design Report for the Phase-II Upgrade of the ATLAS TDAQ System,” CERN-LHCC-2017-020 (2022), [10.17181/CERN.2LBB.4IAL](https://arxiv.org/abs/10.17181/CERN.2LBB.4IAL).
- [164] L. Heinrich, “lukasheinrich/pylhe v0.0.4,” (2018), [10.5281/zenodo.1217032](https://arxiv.org/abs/10.5281/zenodo.1217032).

APPENDIX

This Appendix provides supplementary details supporting the main text. Section 1 provides further methodological details on the simulation of signal and background processes. Section 2 expands the discussion on theoretical systematic uncertainties. Section 3 shows validation studies for generator-level distributions.

1. Technical simulation details

For the elastic $\gamma\gamma \rightarrow \tau\tau$ process, we generate around 2 million MC events for each coupling variation and require $p_T^\tau > 15$ GeV in MADGRAPH by setting `{15:15}=pt_min_pdg` in the `run_card` to improve generator statistics. The SM cross-section reduces from 150 pb to 0.72 pb after imposing $p_T^\tau > 15$ GeV, corresponding to an efficiency of 0.5%. We further improve generator statistics by requiring tau-leptons decay fully leptonically in PYTHIA 8.306 [141, 142] using:

```
15:onMode = off
15:onIfAny = 11 13.
```

We then account for the dileptonic branching fraction $\mathcal{B}(\tau\tau \rightarrow \ell\nu\ell\nu) \simeq 12.4\%$ in cross-section normalization. For elastic processes, the physical picture of the $q_\gamma \rightarrow 0$ limit is that the EM fields surrounding the protons not only comprise the photons pair creating tau-leptons but also provide the quasi-static external EM field in which we measure the tau-lepton EM dipoles.

Single dissociation (elastic-inelastic photon fusion $pp \rightarrow p(\gamma\gamma \rightarrow \tau\tau)p^*$ where one proton dissociates) and double dissociation (inelastic-inelastic photon fusion $pp \rightarrow p^*(\gamma\gamma \rightarrow \tau\tau)p^*$ where both protons dissociate) processes are not implemented in the GAMMAUPC 1.0 package inside MADGRAPH 3.5.0. Therefore, we use MADGRAPH 2.6.7 based on Ref. [91] to implement the equivalent photon approximation [139] prescription for the elastic photon γ , and the default NNPDF23_LO_AS_0130_QED parton distribution functions (PDF) [144] for the inelastic photon γ^* . We find the MADGRAPH cross-section for single (double) dissociative photon-fusion production of tau pairs to be 3.41 pb (2.58 pb) with a $p_T^\tau > 15$ GeV generator requirement. For the $\gamma\gamma \rightarrow WW$ process, no generator cuts are imposed and we find the elastic (single dissociative) cross-section to be 74.1 fb (592 fb). To decay, shower and hadronize such processes, we use PYTHIA configured specifically for photon-fusion processes generated in MADGRAPH. The full PYTHIA settings follow Refs. [91, 143]:

- `PartonLevel:ISR = off` for elastic processes;
- `BeamRemnants:unresolvedHadron` set to 0, 1/2, 3 for elastic, forward/backward single dissociation and double dissociation, respectively;
- All dissociation samples apply these settings:
`PartonLevel:ISR = on`

```
BeamRemnants:primordialKThard = 1.5
BeamRemnants:primordialKTremnant = 0.1
SpaceShower:dipoleRecoil = on
SpaceShower:pTmaxMatch = 0
SpaceShower:pTmaxFudge = 1.0
SpaceShower:pTdampMatch = 1
SpaceShower:pTdampFudge = 1.5
```

For other non-photon-induced background processes, we generate the Drell-Yan $qq \rightarrow Z^{(*)}/\gamma^* \rightarrow \tau\tau$ (which we also denote $qq \rightarrow \tau\tau$ in the main text) and diboson $qq \rightarrow WW \rightarrow \ell\nu\ell\nu$ processes to leading order using MADGRAPH 3.5.0. We employ the default NN23LO PDFs [144] with up to one parton in the matrix element interfaced to PYTHIA for parton shower and hadronization using MLM jet-parton matching [145] with merging scale `xqcut` set to 25 GeV. To improve generator statistics, we decay the tau-leptons leptonically $\tau \rightarrow \ell\nu\nu$ for $\ell \in [e, \mu]$ and impose a generator-level $p_T^\ell > 5$ GeV cut in MADGRAPH (`5=pt1` in `run_card`). After such requirements, the cross-section for these Drell-Yan (diboson) samples is 154 pb (12.6 pb). Top quark pair production is observed to be negligible in $e\mu$ selections after track-vertex isolation [90, 91] given the high track multiplicities of the two heavy-flavor jets, so we avoid simulating this.

2. Theoretical systematic uncertainties

For the $\gamma\gamma \rightarrow \tau\tau$ signal, the elementary cross-section is crucially well predicted by quantum electrodynamics and we expect the dominant modeling uncertainties arise from the photon flux and rescattering effects involving the outgoing protons called soft survival. Uncertainties in the GAMMA-UPC photon flux can be theoretically estimated using alternative form factors such as the Electric Dipole (EDFF) model studied in Ref. [140], which shows our baseline (ChFF) more accurately models the data but has a slightly harder p_T^τ and $m_{\tau\tau}$ spectrum than the other photon-flux models. For $pp \rightarrow p(\gamma\gamma \rightarrow \tau\tau)p$ with $p_T^\tau > 15$ GeV, we find using EDFF gives a cross-section of 0.594 pb that is 18% smaller than our ChFF baseline of 0.720 pb. We also compare these kinematic differences in Fig. 7, which provides a quantitative indication of the theoretical modeling in state-of-the-art generators. We find these discrepancies are within 10% for $m_{\tau\tau} \lesssim 200$ GeV and $p_T^\tau \lesssim 100$ GeV, but grow to higher values reaching over 30%. Further estimation of theoretical uncertainties could be made by comparing with alternative generators such as SUPERCHIC [153]. Dissociative processes additionally have uncertainties arising from the inelastic photon PDF, where we could use alternative PDF sets such as MMHT2015QED_NLO [159]. Precise evaluation of these systematic uncertainties is beyond the scope of this phenomenological study. The main text instead discusses in detail the strategies to experimentally constrain these in situ with data to what we expect to reach percent-level accuracy.

3. Generator-level validation studies

This section provides further kinematic validation of the simulated Monte Carlo samples, specifically the generator-level (also called “truth-level” in the literature) distributions, inspecting the Les Houches Events (LHE) files using PYLHE [164].

To highlight the principal advantage of proton-proton over lead-ion collisions, Fig. 5 illustrates kinematic distributions of the $NN \rightarrow N(\gamma\gamma \rightarrow \tau\tau)N$ process for three beam types N alongside their corresponding center-of-momentum energies (per nucleon for ions): proton-proton pp (14 TeV), proton-lead pPb (8.8 TeV), lead-lead PbPb (5.52 TeV). We normalize the distributions to unity to compare shapes for the ditau invariant mass $m_{\tau\tau}$, tau-lepton transverse momentum p_T^τ and rapidity η_τ . These variables follow the photon flux distributions, where we consider the charged form factor (ChFF) from GAMMA-UPC in MADGRAPH. The pp collisions reach far higher values in $m_{\tau\tau}$ and p_T^τ compared those with lead ions. Relative to $m_{\tau\tau} = 30$ GeV, the $m_{\tau\tau}$ spectrum drops by four orders of magnitude at 200 GeV, 400 GeV and 1000 GeV for PbPb, pPb and pp, respectively. Similarly, the p_T^τ spectrum for pp is significantly harder compared to PbPb, where the p_T^τ can probe above 200 GeV for pp that is inaccessible to PbPb. Moreover, the tau-leptons in elastic production are back-to-back in the transverse plane with little transverse boost of the ditau system, so the kinematic boost of the individual tau-leptons arises from the center-of-mass system of the initial-state photons. The η_τ distribution highlights how the larger beam energy of pp gives a higher longitudinal boost than PbPb, while the pPb verifies the expected asymmetric distribution, which illustrate suitability for the LHCb experimental acceptance $2 < |\eta| < 5$ and upgraded trackers for ATLAS and CMS covering $|\eta| < 4$.

We study the impact of the different LHC pp center-of-mass energies $\sqrt{s} \in \{13, 13.6, 14\}$ TeV on distributions of the $pp \rightarrow p(\gamma\gamma \rightarrow \tau\tau)p$ process in Fig. 6. This illustrates the differences in \sqrt{s} are generally small within the scope of this study. Therefore for simplicity, we generate samples at only 14 TeV and rescale luminosities to estimate LHC and HL-LHC sensitivity in the main text. This is only relevant in the short term where we anticipate the ATLAS and CMS collaborations would combine the 13 TeV from Run 2 with the 13.6 TeV dataset from Run 3, while HL-LHC is expected to reach 14 TeV. Crucially, the slight suppression in rate for 13 TeV compared to 14 TeV at the highest $m_{\tau\tau}$ bins are around $\mathcal{O}(10\%)$, which remain subdominant compared to the suppression when using lead ion fluxes (Fig. 5). The suppression at the highest $|\eta_\tau|$ values is expected for the reduced longi-

tudinal boost of smaller beam energies, but are outside the close to negligible for the $|\eta| < 4$ acceptance of the upgraded ATLAS and CMS tracker.

To estimate theoretical uncertainties of the photon flux, Fig. 7 shows the impact on tau-lepton kinematics when considering an alternative photon flux denoted the Electric Dipole form factor (EDFF) in the GAMMA-UPC package. In Ref. [140], the differences from the ChFF nominal we adopt in this paper are discussed and compared with dielectron and dimuon measurements. In brief, they found the ChFF flux provides better differential modelling but slightly overestimates the data by around 10% compared with the EDFF flux. We find differences of around 10 to 20% at high $m_{\tau\tau}$ and 20 to 30% for p_T^τ tails. Fortunately, experimental analyses can constraint these differences using data-driven control sample techniques as discussed in the main text. We expect future measurements of dilepton standard candles and theoretical work will improve these theoretical uncertainties.

Figure 8 shows how shifts in magnetic dipole moments δa_τ impact tau-lepton kinematics. These shape differences are modest in the $m_{\tau\tau}$ and especially striking in the p_T^τ spectra, rising at high values as expected from effective field theory. Changes in these spectra also modify the kinematics of the tau-lepton decay products. Analyses can therefore fit observables such as the electron and muon p_T^ℓ spectra in $\tau \rightarrow \ell\nu\nu$ decays to substantially enhance sensitivity to δa_τ beyond measuring inclusive cross-sections alone, as introduced in Ref. [49].

Figure 9 compares how SM, BSM-only and their combined (SM + BSM) diagrams in the matrix elements impact unit-normalized differential distributions of $m(\tau\tau)$ and p_T^τ . To generate only the linear (quadratic) pieces with one (two) BSM dipole vertices entering the matrix element, we set $NP^2=1$ ($NP^2=2$) in MADGRAPH. Displayed are shifts in the magnetic dipole of $\delta a_\tau = 0.01$.

Figure 10 shows the enlarged and zoomed axis versions of Fig. 2 for the $\gamma\gamma \rightarrow \tau\tau$ cross-section varying with magnetic dipole shifts δa_τ assuming $\delta d_\tau = 0$. This highlights the dramatic impact on the cross-section variations $\sigma_{\gamma\gamma \rightarrow \tau\tau} / \sigma_{\gamma\gamma \rightarrow \tau\tau}^{\text{SM}}$ as we consider tighter requirements on $p_T^\tau > 3, 30, 100$ GeV, reserving the 100 GeV requirement only for pp. By contrast, for a given minimum p_T^τ , the different beam types with corresponding center-of-mass energies (pp, pPb, PbPb) have a subdominant effect. For $p_T^\tau > 3, 30$ GeV, the cross-section changes by less than 1% for $-0.003 < \delta a_\tau < 0.002$, whereas imposing $p_T^\tau > 100$ GeV provides a percent-level cross-section change even for shifts below per-mille $-0.0008 < \delta a_\tau < 0.0007$. Table I display the absolute total LHC cross-sections of elastic $\gamma\gamma \rightarrow \tau\tau$ production when varying the magnetic δa_τ . This considers various beam configurations and generator requirements on the tau-lepton transverse momentum.

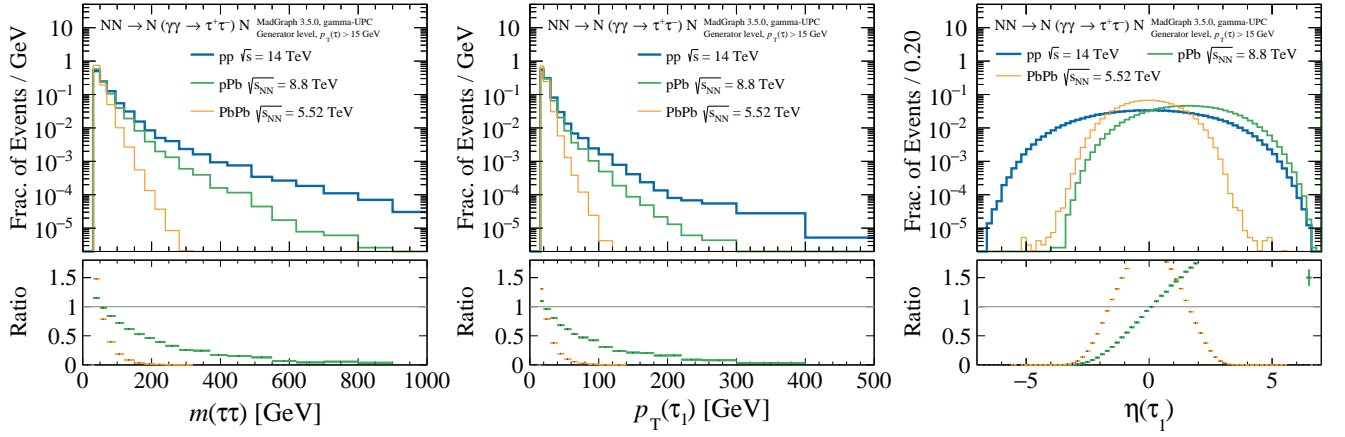


FIG. 5. Unit normalized generator-level MADGRAPH distributions of $\gamma\gamma \rightarrow \tau\tau$ comparing beam types: pp (thin blue), proton-lead pPb (medium green), lead-lead PbPb (thick orange). A generator-level requirement of $p_T(\tau) > 15$ GeV is imposed using the charged form-factor photon flux from GAMMA-UPC. The lower panel shows the ratio relative to the nominal pp .

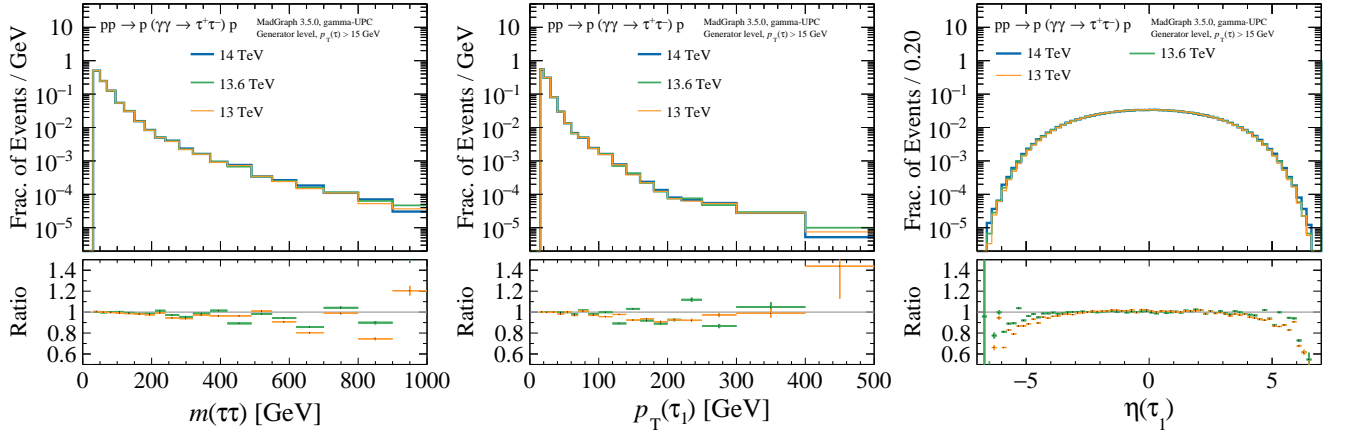


FIG. 6. Unit normalized generator-level MADGRAPH distributions of $\gamma\gamma \rightarrow \tau\tau$ comparing pp centre-of-mass energy: 14 TeV (thick blue), 13.6 TeV (medium green), 13 TeV (thin orange). A generator-level requirement of $p_T(\tau) > 15$ GeV is imposed using the charged form-factor photon flux from GAMMA-UPC. The lower panel shows the ratio relative to the nominal 14 TeV.

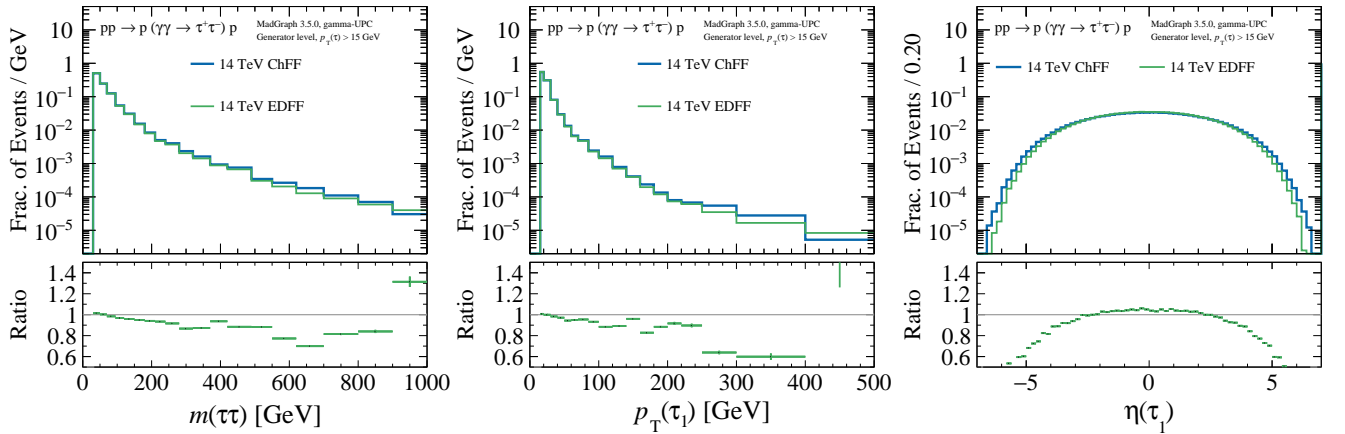


FIG. 7. Unit normalized generator-level MADGRAPH distributions of $\gamma\gamma \rightarrow \tau\tau$ comparing pp at 14 TeV photon flux choices of GAMMA-UPC in MADGRAPH: charged form factor “ChFF” (thick blue), electric dipole form factor “EDFF” (medium green). A generator-level requirement of $p_T(\tau) > 15$ GeV is imposed. The lower panel shows the ratio relative to the nominal ChFF.

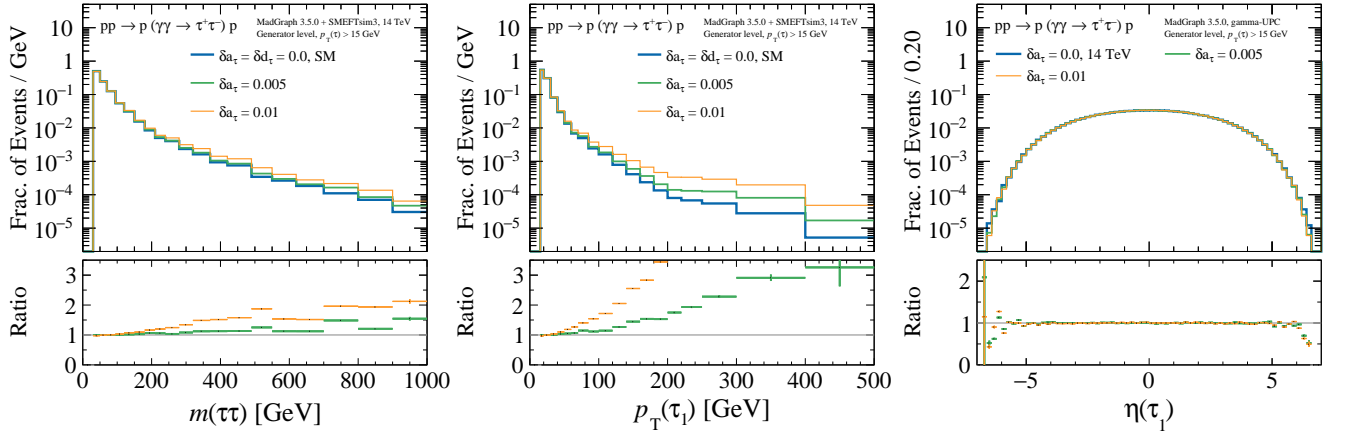


FIG. 8. Unit normalized generator-level MADGRAPH distributions of $\gamma\gamma \rightarrow \tau\tau$ comparing magnetic dipole variations δa_τ (upper) for pp at 14 TeV photon flux choices of GAMMA-UPC in MADGRAPH. A generator-level requirement of $p_T(\tau) > 15$ GeV is imposed. The lower panel of each subfigure shows the ratio relative to the SM nominal.

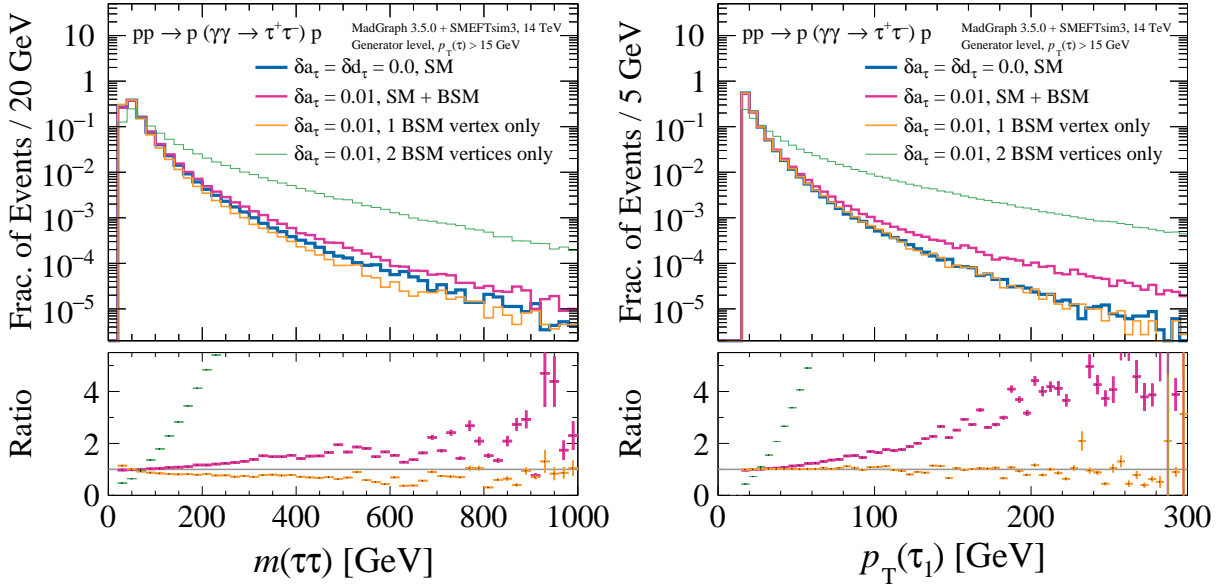


FIG. 9. Unit normalized generator-level MADGRAPH distributions of $pp \rightarrow p(\gamma\gamma \rightarrow \tau\tau)p$ at 14 TeV comparing the SM-only (very thick blue), SM plus BSM ($NP^2 \leq 2$, thick pink), only 1 BSM vertex ($NP^2 = 1$, medium orange), only 2 BSM vertices ($NP^2 = 2$, thin green) for $\delta a_\tau = 0.01$. A generator-level requirement of $p_T^\tau > 15$ GeV is imposed. The lower panel shows the ratio relative to the SM nominal.

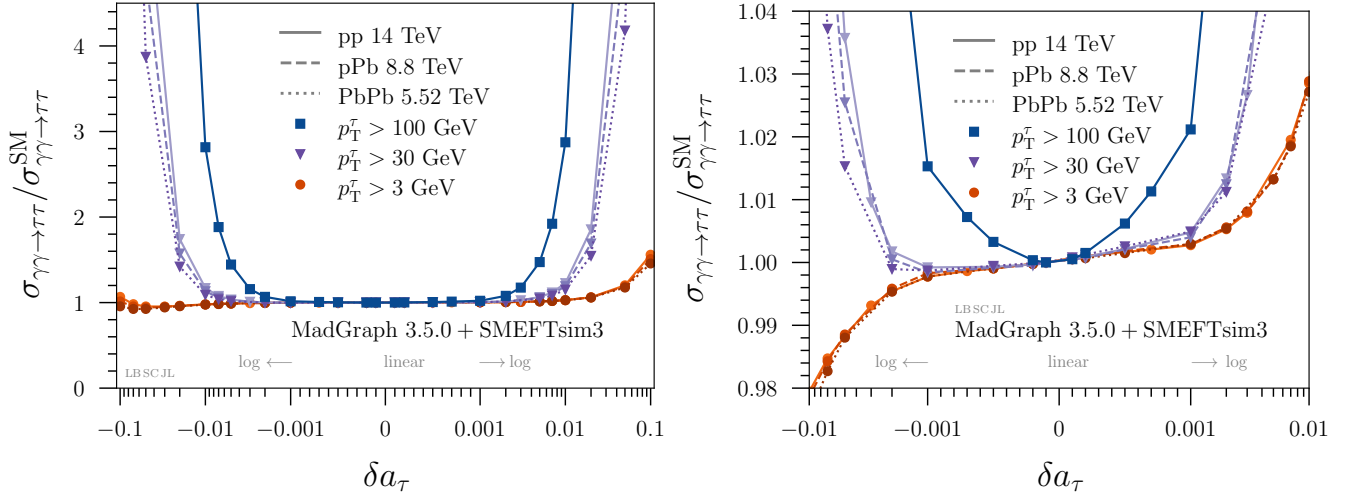


FIG. 10. Wider (left) and zoomed (right) axis version of Fig. 2 showing cross-sections relative to the SM computed using MADGRAPH+SMEFTSIM for elastic photon-fusion production of tau-lepton pairs $\sigma_{\gamma\gamma\rightarrow\tau\tau}/\sigma_{\gamma\gamma\rightarrow\tau\tau}^{\text{SM}}$ vs magnetic moment variations δa_τ . Various beam types and center-of-mass energies are displayed: proton-proton pp 14 TeV (solid), proton-lead pPb 8.8 TeV (dashed), lead-lead PbPb 5.52 TeV (dotted). Different generator requirements on the minimum tau-lepton transverse momentum p_T^τ are shown: 100 GeV (blue squares, only pp), 30 GeV (purple triangles), 3 GeV (orange circles). Note the linear-log scale division at $\delta a_\tau = \pm 0.001$.

$\sigma_{\gamma\gamma\rightarrow\tau\tau}^{\text{LHC}}$ [pb]:	pp 14 TeV	pPb 8.8 TeV	PbPb 5.52 TeV	pp 14 TeV	pPb 8.8 TeV	PbPb 5.52 TeV	pp 14 TeV
δa_τ	$p_T^\tau > 3 \text{ GeV}$	$p_T^\tau > 3 \text{ GeV}$	$p_T^\tau > 3 \text{ GeV}$	$p_T^\tau > 30 \text{ GeV}$	$p_T^\tau > 30 \text{ GeV}$	$p_T^\tau > 30 \text{ GeV}$	$p_T^\tau > 100 \text{ GeV}$
0.1	61.27	1.499×10^5	2.35×10^8	2.181	2047	3.454×10^5	0.4644
0.05	47.23	1.181×10^5	1.896×10^8	0.628	610.5	1.076×10^5	0.1179
0.02	41.74	1.054×10^5	1.707×10^8	0.1901	202.4	3.978×10^4	0.02109
0.01	40.41	1.022×10^5	1.657×10^8	0.1256	142.6	2.963×10^4	0.007192
0.005	39.76	1.007×10^5	1.634×10^8	0.109	126.3	2.69×10^4	0.003687
0.002	39.5	9.991×10^4	1.622×10^8	0.1038	121.2	2.602×10^4	0.0027
0.001	39.4	9.964×10^4	1.618×10^8	0.1029	120.2	2.586×10^4	0.002556
0.0	39.22	9.933×10^4	1.611×10^8	0.1024	120	2.581×10^4	0.002505
-0.001	39.21	9.918×10^4	1.609×10^8	0.1023	119.5	2.57×10^4	0.002541
-0.002	39.12	9.894×10^4	1.605×10^8	0.1026	119.8	2.57×10^4	0.002671
-0.005	38.83	9.821×10^4	1.594×10^8	0.1061	122.8	2.613×10^4	0.003615
-0.01	38.49	9.723×10^4	1.574×10^8	0.1198	135.6	2.806×10^4	0.007048
-0.02	37.82	9.547×10^4	1.544×10^8	0.1784	188.4	3.655×10^4	0.02079
-0.05	37.52	9.356×10^4	1.493×10^8	0.5982	575.6	9.965×10^4	0.1172
-0.1	41.91	1.007×10^5	1.542×10^8	2.119	1977	3.294×10^5	0.4627

TABLE I. Generator-level LHC cross-sections $\sigma_{\gamma\gamma\rightarrow\tau\tau}^{\text{LHC}}$ in picobarns (pb) for elastic photon-fusion production of tau-lepton pairs using MADGRAPH 3.5.0 and the charged form factor photon fluxes from GAMMA-UPC. This is interfaced with the SMEFTSIM3 package to evaluate for variations in the anomalous magnetic moment δa_τ . The columns show different beam species with their corresponding center-of-mass energies, and different generator-level requirements on the tau-lepton transverse moment p_T^τ .